

Magnesium and Magnesium-Silicide coated Silicon Nanowire composite Anodes for Lithium-ion Batteries

Alireza Kohandehghan^{a,b}, Peter Kalisvaart^{a,b,*}, Martin Kupsta^b, Benjamin Zahiri^{a,b}, Babak Shalchi Amirkhiz^{a,b}, Zhipeng Li^c, Elmira L. Memarzadeh^{a,b}, Leonid A. Bendersky^c, David Mitlin^{a,b,**}

^a: University of Alberta, Chemical&Materials Engineering, 9107 116th street, T6G 2V4, Edmonton AB, Canada

^b: National Research Council, National Institute for Nanotechnology, Edmonton, Alberta T6G 2M9, Canada

^c: Material Science and Engineering Division, Material Measurement Laboratory, National Institute of Standards and Technology, Gaithersburg MD 20899 USA

* pkalisvaart@gmail.com and ** dmitlin@ualberta.ca

Supporting information

Figure S1 (a) shows a cross-sectional view of SiNWs grown on a Si wafer with Ti and TiN barrier layers. In their as-grown state, the nanowires are maximum 15 micrometers tall with an average of approximately 12 microns. Figure S1 (b-d) show representative plane-view images of bare SiNWs, (b), nanowires coated with 10 nm Mg, (c), and nanowires where the Mg has been reacted to Mg₂Si, (d). From these images, the distributions of the projected diameters of the nanowires were obtained as shown in Figure S1 (e). The bare SiNWs have an average diameter of 114 nm, which is close to the value of 105 nm reported before²⁸. It should be noted here that the cross-section of the SiNWs is not perfectly circular but hexagonal, as is shown in Figure S3. Hence the use of the term *projected* diameter.

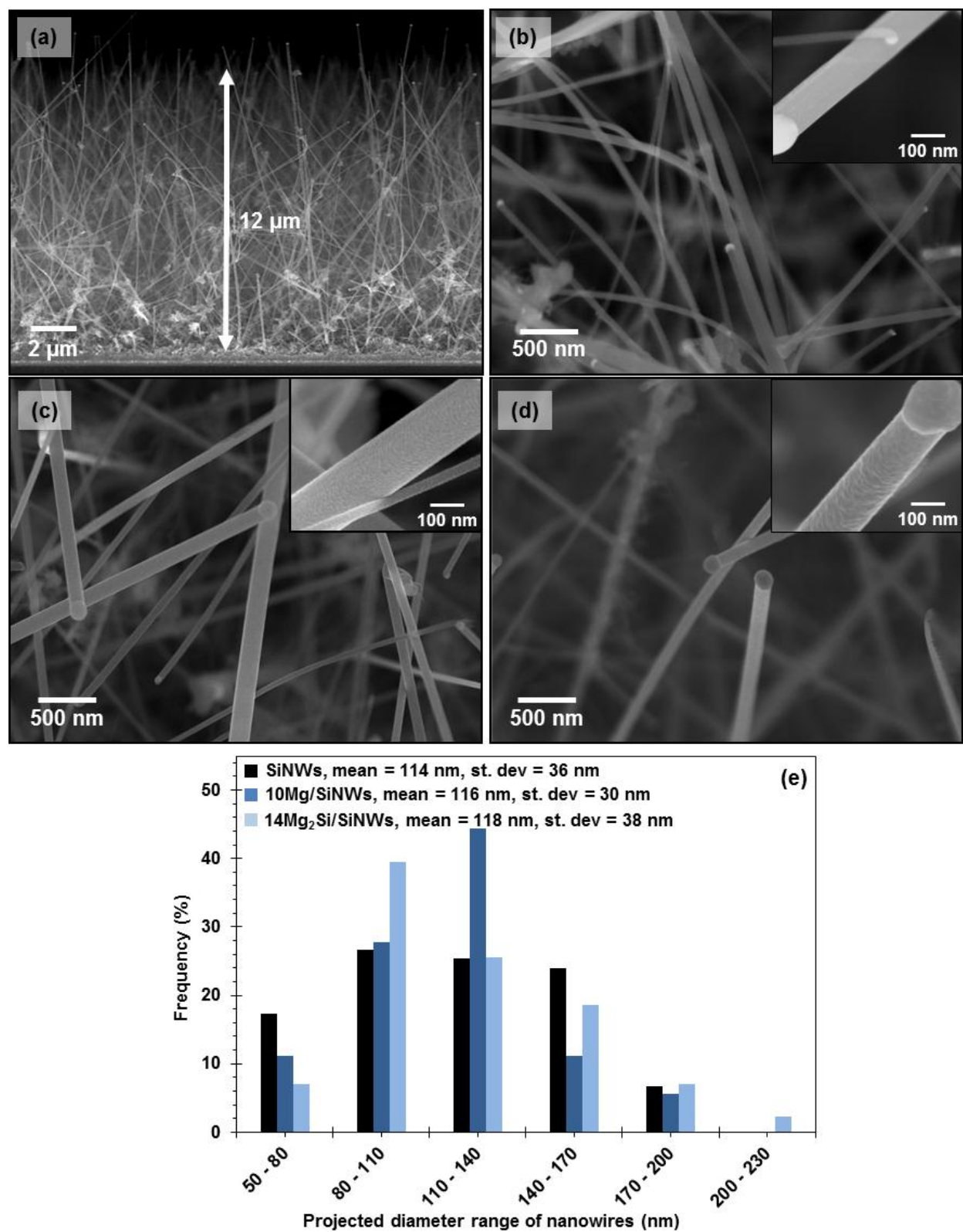


Figure S1. (a) SEM micrograph of SiNW forest grown on Si/Ti/TiN, cross-sectional view, (b) bare SiNWs in-plane view, (c) and (d) same as (b) for 10Mg/SiNWs and 14Mg₂Si/SiNWs. A series of representative images like (b)-(d) were used to obtain the diameter distribution in (e).

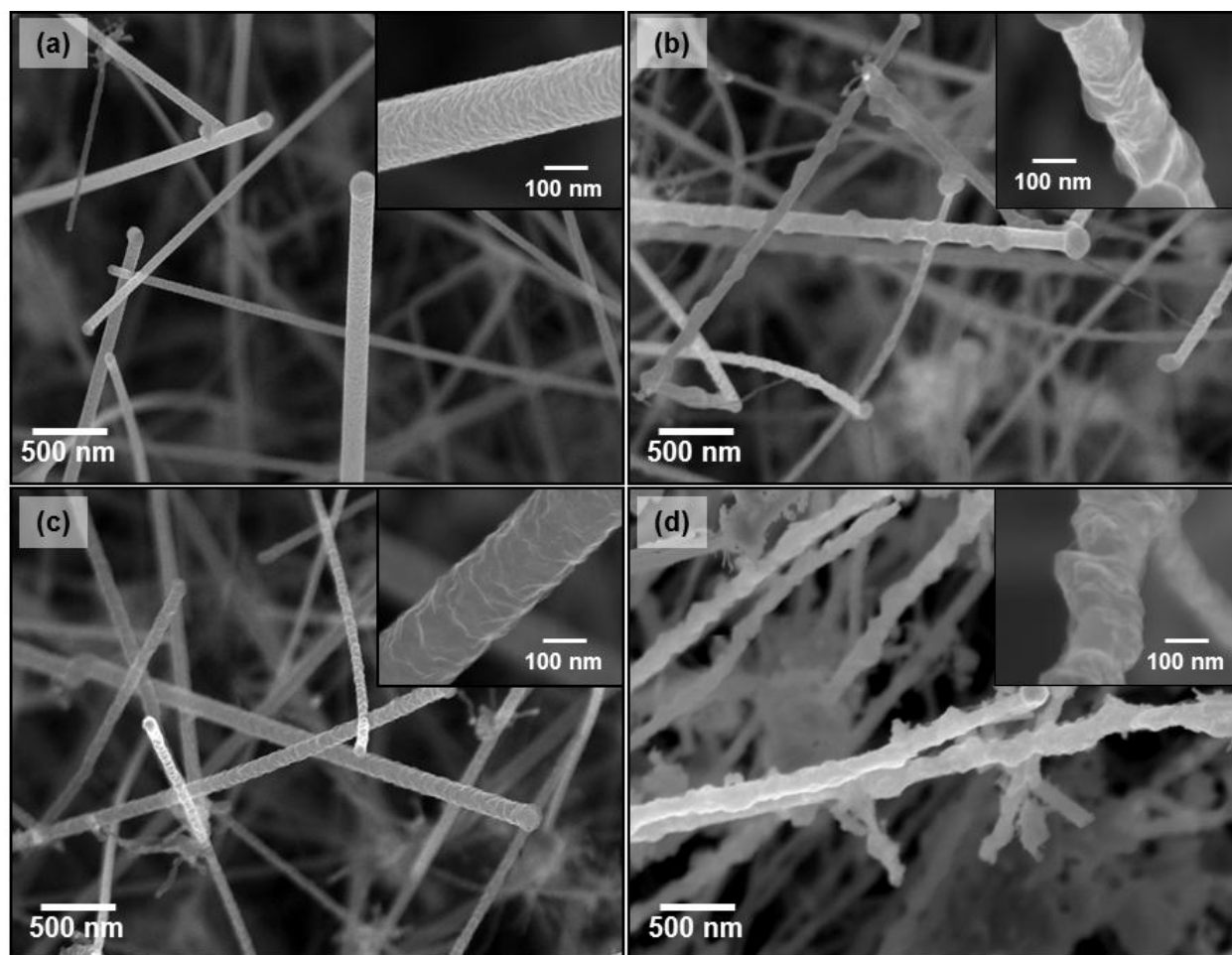


Figure S2. SEM micrographs and high magnification close-up (insert) of as-synthesized (a) 20Mg/SiNWs, (b) 28Mg₂Si/SiNWs, (c) 50Mg/SiNWs, and (d) 70Mg₂Si/SiNWs nanocomposite anode materials.

Figure S2 displays SEM micrographs of as-synthesized Mg/SiNWs and Mg₂Si/SiNWs structures with equivalent geometrical Mg thicknesses for thicker Mg. Panels (a) and (b), (c) and (d), represent the same material before and after annealing. The 20Mg/SiNWs, shown in Figure S2 (a), still have a relatively smooth surface and quite homogenous diameters with catalyst particles on the tips, indicating tip growth mechanism. Comparing Figure S2 (a) and (b), we can see that annealing increases the surface roughness upon reacting the Mg with the underlying Si to Mg₂Si. For higher loadings, this effect becomes even stronger.

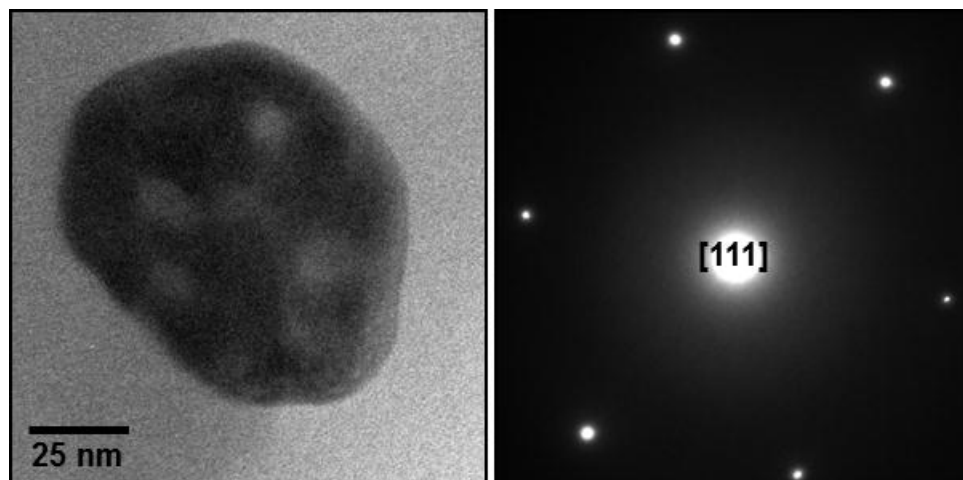


Figure S3. Cross-section bright-field micrograph of a silicon nanowire and corresponding SAD pattern showing that the imaged SiNW is oriented near the 111 zone axis.

Figure S3 shows a cross-sectional bright-field image of a single silicon nanowire. From the SAD pattern, it is clear that the nanowire is oriented near its 111 zone-axis. What was not entirely clear from the SEM images in Figure S1 is that the nanowire cross-section is not circular, but is instead shaped like a slightly irregular hexagon. Hence the term ‘projected diameter’ in Figure S1 (e).

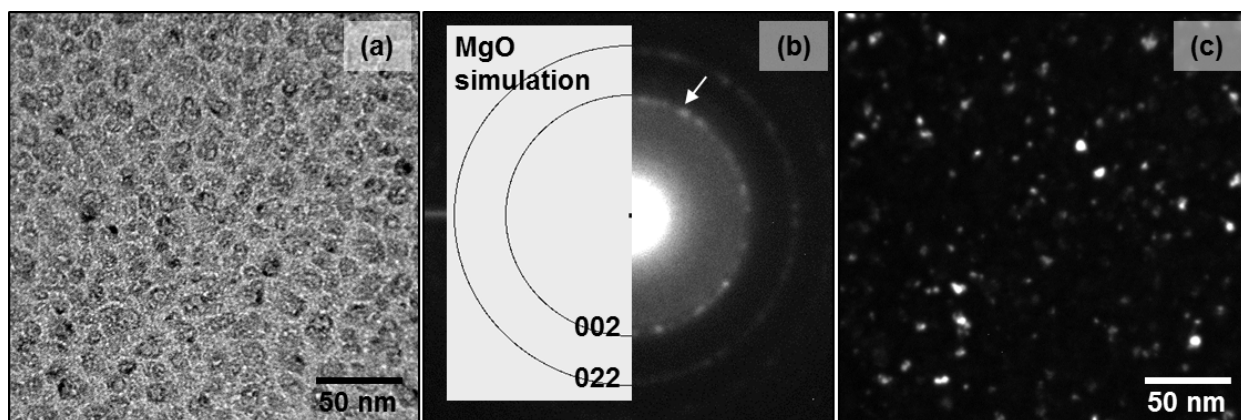


Figure S4. TEM images of sputtered 10 nm Mg onto a TEM grid (on the Cu side) at room temperature, (a) bright-field, (b) corresponding SAD pattern, and (c) dark-field TEM micrograph, obtained using part of 002_{MgO} diffracted ring. This thin Mg layer appears mostly oxidized, as it did on the composite

For the thinnest Mg coating, it was shown in Figure 1 (e-h) that all Mg is likely oxidized upon exposure to air after synthesis. This is confirmed in Figure S4 which is a TEM image of a 10 nm planar Mg film deposited onto a TEM grid. The film indeed appears to consist of mainly MgO.

X-ray diffraction (XRD) characterizations using Cu-K α radiation ($\lambda=1.5406$ Å), monochromatized by a single Göbel mirror, were conducted on a Bruker AXS diffractometer (Bruker Discover 8). The diffractometer is equipped with a HiStar general area 2-dimensional detection system (GADDs) with sample-detector distance of 15 cm. Phase identification has been performed employing the XRD database on EVA software.

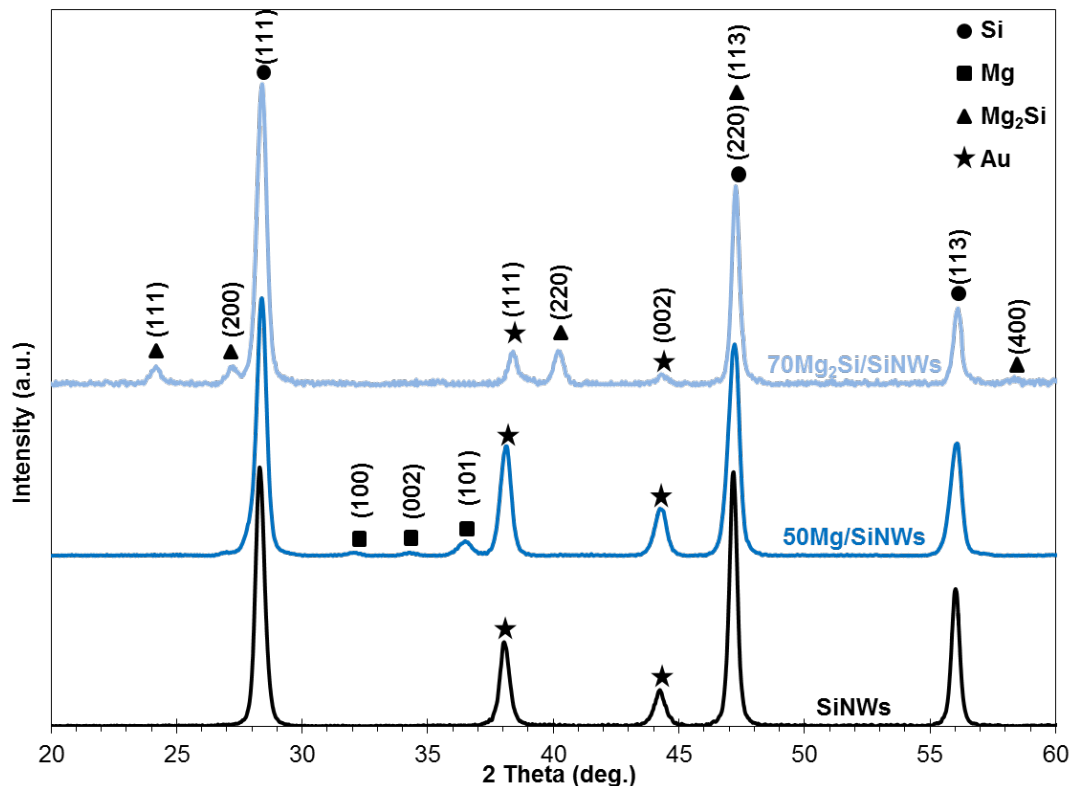


Figure S5. XRD patterns of bare SiNWs, 50Mg/SiNWs and 70Mg₂Si/SiNWs made by annealing 50Mg/SiNWs at 400 °C for 30 minutes.

Figure S5 shows the XRD pattern of bare SiNWs, 50Mg/SiNWs and 70Mg₂Si/SiNWs made by annealing 50Mg/SiNWs for 30 minutes at 400 °C, all grown on a TiN-coated (100) Si wafer. It

should be noted that the synthesized structures were scraped off the Si wafer and then XRD experiments were conducted. The pattern for the bare SiNWs shows the (111), (220) and (311) reflections of Si as well as two clear peaks of the Au catalyst. Metallic Mg is clearly present in 50Mg/SiNWs and after annealing, several of the strongest reflections of the Mg_2Si phase are visible in the diffraction pattern, confirming reaction of the Mg coating with Si during heat treatment.

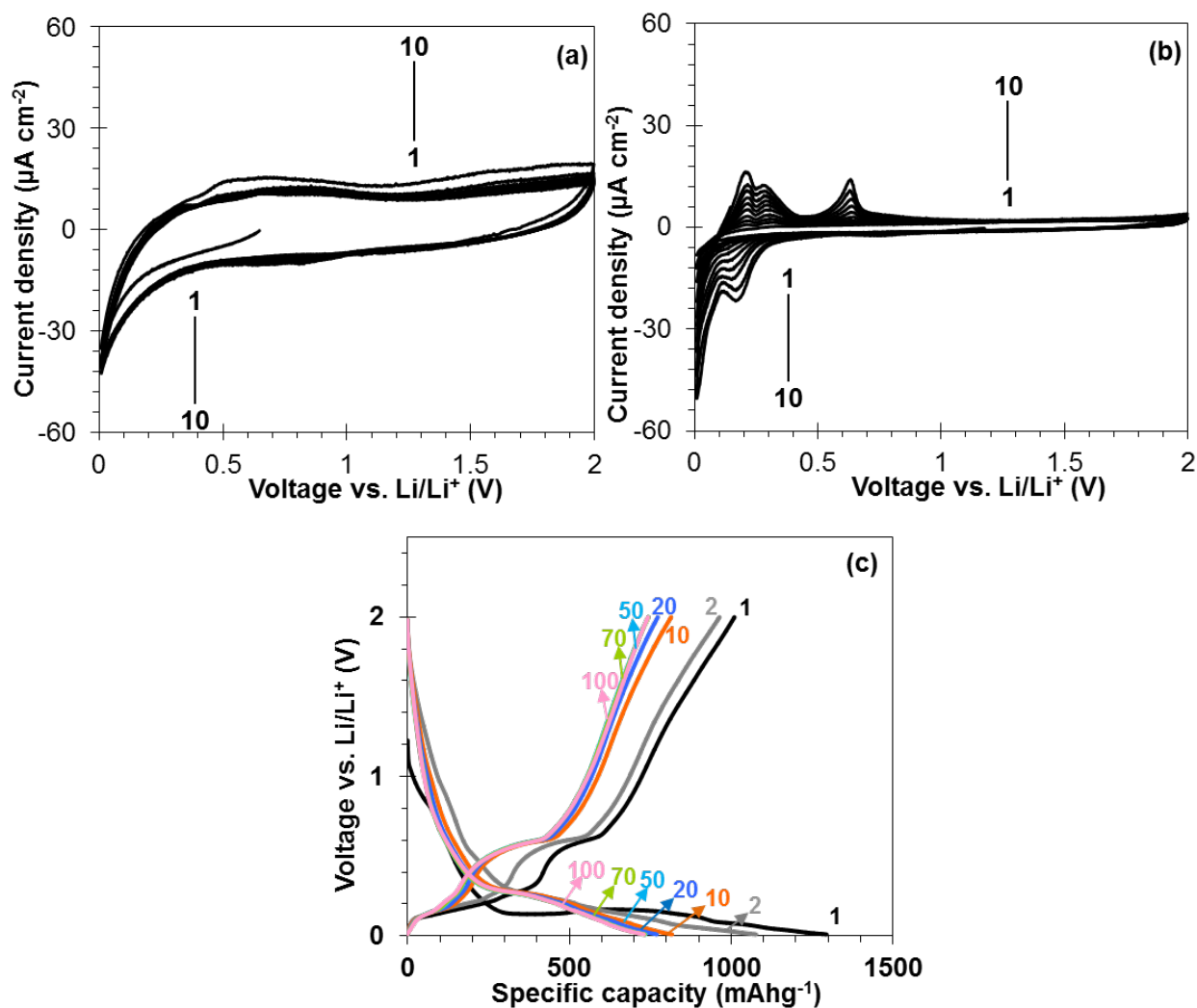


Figure S6. (a) and (b) CV curves between 0 and 2 V vs. Li/Li⁺ for a planar 100 nm Mg_2Si layer at 1 and 0.2 mV/s, respectively, (c) CC cycling at 0.1C rate of the same over the same potential window.

Cyclic voltammetry curves and constant-current charge-discharging of a 100 nm Mg_2Si film are shown in Figure S6. Note that the scanning rate had to be lowered to 0.2 mV/s in order to see any distinct features in the CV curves, indicating poor reaction kinetics. The capacity in the CC measurements is, at $\sim 1300 \text{ mAhg}^{-1}$, approximately equal to what is found in the literature (see ref. 33)

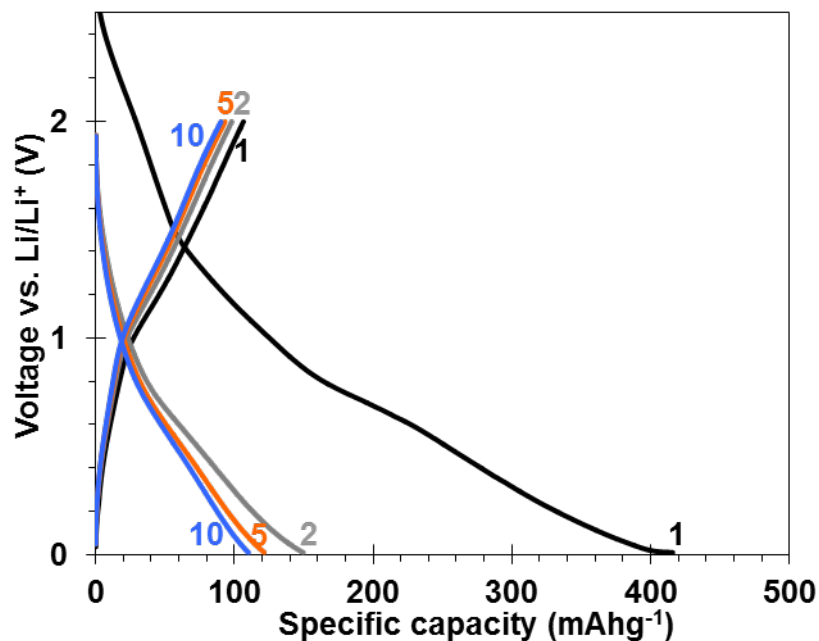


Figure S7. CC measurements on 100 nm planar Mg film at 1 μA current

CC measurements on a planar 100 nm Mg film at very low currents is shown in Figure S7 in order to establish to maximum amount of charge that can be stored in Mg. On the first lithiation, $\sim 400 \text{ mAhg}^{-1}$ is stored, but this quickly decreases to 100. This shows it is unlikely that the Mg metal coating on the SiNWs stores a significant amount of Li during cycling.

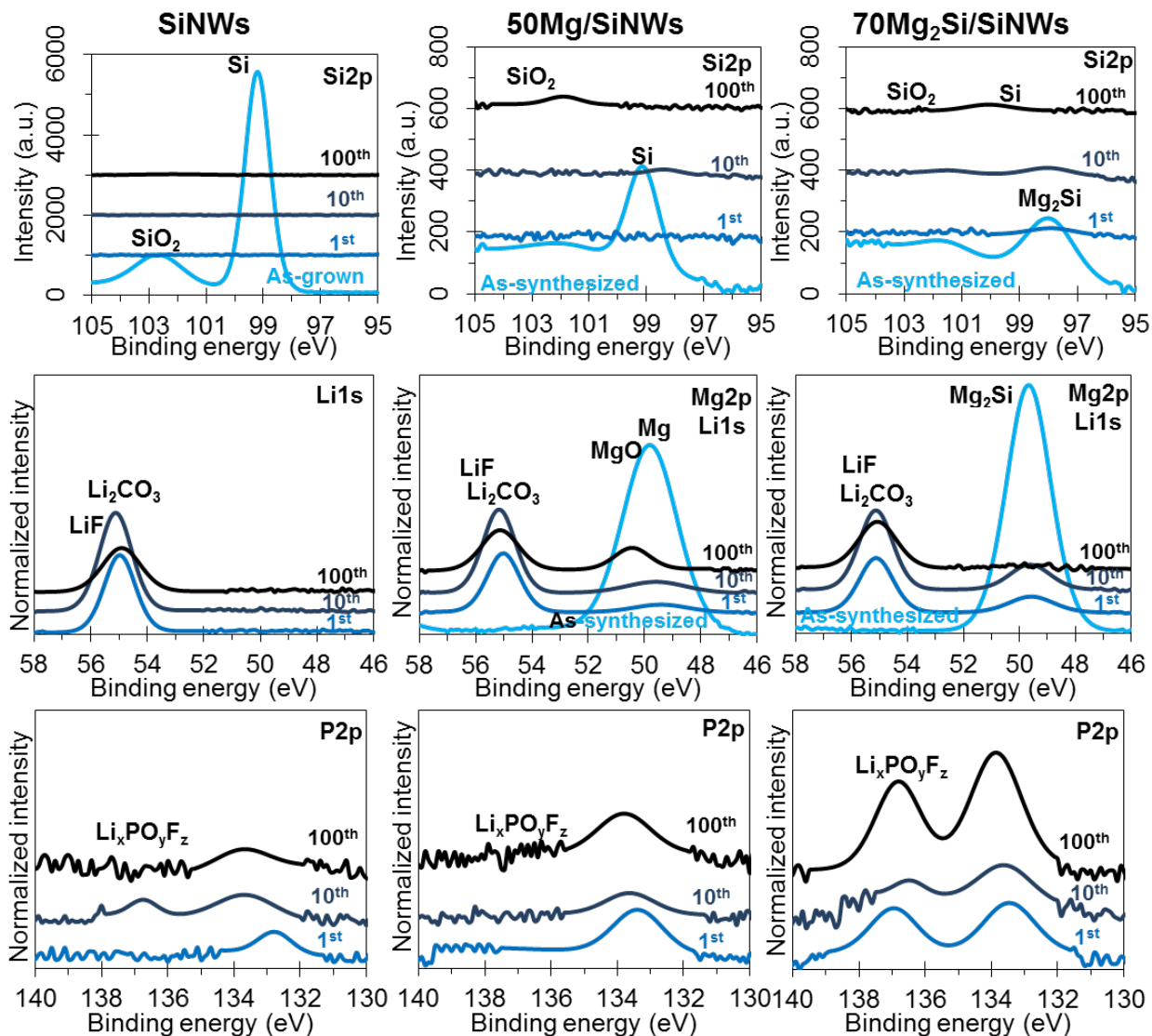


Figure S8. XPS spectra for Si_{2p}, Li_{1s}/Mg_{2p}, and P_{2p} for as-made and cycled bare SiNWs, 50Mg/SiNWs, and 70Mg₂Si/SiNWs taken from the top of the nanowire forest.

The Si_{2p}, Li_{1s}/Mg_{2p}, and P_{2p} XPS spectra for bare and Mg- and Mg₂Si-coated nanowires are shown in Figure S8. As in the O_{1s} spectra in Figure 10, the presence of native oxide in the as-made electrodes is obvious. After the first cycle, this oxide is either covered by SEI or reduced. In the Li_{1s} spectra, the peak for LiF overlaps strongly with that of Li₂CO₃, but there is considerable intensity in the energy range where the LiF peak would be expected in all spectra. Combined with the F_{1s} spectra, where the peak for LiF is much more easily resolved, the

presence of LiF is unambiguous and the differences in the amounts of LiF in the different electrodes can therefore be deduced from the F1s spectra in Figure 10. The intensity of the broad peak around 137 eV in the P2p spectra for 70Mg₂Si/Si NWs seems to correlate with the intensity of the shoulder at 687 eV in the F1s spectra in Figure 10, indicating that it is also related to the Li-P-O-F decomposition product of the electrolyte salt.